7584 *Biochemistry* **2009,** *48,* 7584–7594
DOI: 10.1021/bi9009264

BIOCHEMISTRY
including biophysical chemistry & molecular biology
Article

Kinetic Intermediate Reveals Staggered pH-Dependent Transitions along the Membrane Insertion Pathway of the Diphtheria Toxin T-Domain†

Alexander Kyrychenko,‡ Yevgen O. Posokhov,‡ Mykola V. Rodnin, and Alexey S. Ladokhin*

Department of Biochemistry and Molecular Biology, Kansas University Medical Center, Kansas City, Kansas 66160-7421 ‡Permanent address for A.K. and Y.O.P.: Institute for Chemistry, V. N. Karazin Kharkiv National University, 4 Svobody Square, Kharkiv 61077, Ukraine

Received December 1, 2008; Revised Manuscript Received July 8, 2009

ABSTRACT: The pH-triggered membrane insertion pathway of the T-domain of diphtheria toxin was studied using site-selective fluorescence labeling with subsequent application of several spectroscopic techniques (e.g., fluorescence correlation spectroscopy, FRET, lifetime quenching, and kinetic fluorescence). FCS measurements indicate that pH-dependent formation of the membrane-competent form depends only slightly on the amount of anionic lipids in the membrane. The subsequent transbilayer insertion, however, is strongly favored by anionic lipids. Kinetic FRET measurements between the donor-labeled T-domain and acceptor-labeled lipid vesicles demonstrate rapid membrane association at all pH values for which binding occurs. In contrast, the transmembrane insertion kinetics is significantly slower and is also both pH- and lipid-dependent. Analysis of kinetic behavior of binding and insertion indicates the presence of several interfacial intermediates on the insertion pathway of the T-domain, from soluble W-state to transmembrane T-state. Intermediate interfacial I-state can be trapped in membranes with low content of anionic lipids (10%). In membranes of greater anionic lipid content, another pH-dependent transition results in the formation of the insertion-competent state and subsequent transmembrane insertion. Comparison of the results of various kinetic and equilibrium experiments suggests that the pH dependences determining membrane association and transbilayer insertion transitions are different but staggered. Anionic lipids not only assist in formation of the insertion-competent form but also lower the kinetic barrier for the final insertion.

The function of the diphtheria toxin T-domain is to translocate the catalytic domain across the lipid bilayer in response to acidification of the endosome, a task this 178-residue protein is able to perform without the help of any other proteins (*1*). Although the exact mechanism of membrane translocation is not understood, protein refolding in the lipid bilayer environment has to be the central issue. Thus, deciphering the mechanism of pH-triggered DTT[1] insertion is expected to not only impact the field of cellular entry of toxins, many of which also enter the cell via the endosomal pathway (*2*−*4*), but also advance our understanding of general physicochemical principles underlying membrane protein assembly and stability.

The crystallographic structure of DTT in the water-soluble form (*5*) (Figure 1) provides a starting point for refolding/insertion studies. The protein consists of nine helices of various lengths (TH1−9), eight of which completely surround the most hydrophobic one, TH8. Acidification of the endosomal environment results in a conformational change in the T-domain leading to bilayer insertion. Although the insertion pathway is not completely understood on a molecular level, most studies agree that, in the final form, helical hairpin TH8−TH9 adopts a transbilayer conformation with the linker segment translocated to the interfacial region of the *trans* leaflet (*6*−*10*). A number of studies have reported the existence of various noninserted states, which are considered to be insertion/refolding intermediates (*11*−*15*). No direct kinetic study of the insertion pathway, however, has been reported.

Recently, we demonstrated how various spectroscopic techniques can be used to characterize the pH-dependent insertion pathway of another membrane protein, annexin B12 (ANX) (*16*). Here we use these and other methods to follow membrane insertion of the T-domain and compare the obtained results to the hallmarks established with ANX. We use site-directed labeling methodology to introduce into the T-domain specific fluorescence probes suitable for equilibrium and kinetic studies of

†This research was supported by NIH Grants GM-069783 and GM-069783-S1.

*To whom correspondence should be addressed. Phone: 913-588-0489. Fax: 913-588-7440. E-mail: aladokhin@kumc.edu.

[1]Abbreviations: T-domain (or DTT), diphtheria toxin translocation domain; Alexa-labeled T-domain, single-cysteine mutant N235C of the T-domain, labeled with Alexa488 for FCS or FRET measurements of membrane association; DTT-350-NBD, DTT-369-NBD, and DTT-378-NBD, NBD-labeled single-cysteine mutants L350C, Q369C, and P378C of the T-domain used for bilayer insertion measurements (Figure 1); LysoUB, UniBlue-1-palmitoyl-2-hydroxy-*sn*-glycero-3-phosphoethanolamine; NBD, 7-nitrobenz-2-oxa-1,3-diazol-4-yl; FRET, Förster resonance energy transfer; LUV, large unilamellar vesicles; POPC, palmitoyloleoylphosphatidylcholine; POPG, palmitoyloleoylphosphatidylglycerol; 25PC:75PG, 75PC:25PG, and 90PC:10PG, mixtures of POPC and POPG that contain a molar percentage of the corresponding lipid specified by the number; TM, transmembrane; IF, interfacial; F_{MC}, fraction of membrane-competent T-domain; F_{IC}, fraction of insertion-competent T-domain; φ, membrane surface potential; FCS, fluorescence correlation spectroscopy; ANX, annexin B12. Various states along the insertion pathway: W-state, membrane-incompetent aqueous conformation at neutral pH; W^+-state, membrane-competent protonated aqueous conformation; I-state, interfacial intermediate state; I^+-state, insertion-competent protonated state; T-state, transmembrane inserted state.

 Published on Web 07/09/2009

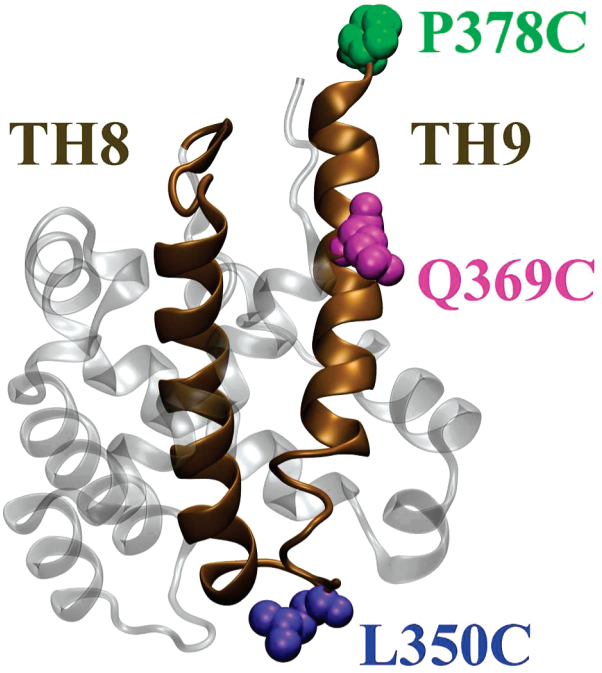

FIGURE 1: Crystallographic structure of the diphtheria toxin T-domain in soluble form at neutral pH (*5*). The consensus insertion hairpin consisting of helices TH8 and TH9 is shown solid, while the rest of the structure is shown semitransparent. Three residues, L350, Q369, and P378 (highlighted in CPK), along TH9 were replaced with cysteines one at a time to provide unique labeling sites for fluorescence dye NBD used in steady-state and kinetic measurements of insertion.

binding and insertion. Our results indicate that the membrane insertion pathway of the T-domain contains several kinetic intermediates and two major pH-dependent steps: formation of the membrane-competent state and of the insertion-competent state. These discrete steps have overlapping pH ranges but varying dependencies on the properties of the lipid bilayer. We demonstrate that anionic lipids play a crucial role in the final stages of insertion by promoting formation of the insertion-competent state on membrane interfaces and by lowering the thermodynamic barriers for transbilayer insertion.

MATERIALS AND METHODS

Materials. Palmitoyloleoylphosphatidylcholine (POPC), palmitoyloleoylphosphatidylglycerol (POPG, and 1,2-dioleoyl-*sn*-glycero-3-phosphoethanolamine-*N*-(lissamine rhodamine B sulfonyl) ammonium salt (Rhodamine-PE) were obtained from Avanti Polar Lipids (Alabaster, AL). UniBlue A vinyl sulfone was purchased from Sigma (St. Louis, MO). IANBD ester, monobromobimane and AlexaFluor-488 maleimide were from Invitrogen (Carlsbad, CA). Labeling with fluorescent dyes was performed using a standard procedure for the thiol-reactive derivatives (*14*, *17*, *18*). Typically, 1 mg of the maleimide derivative of the dye was dissolved in 50 μL of DMFA and added dropwise to the protein solution in PBS (pH 7.4) containing 0.1 mM EDTA. The reaction mixture was incubated for 2 h at room temperature or overnight at 4 °C. Unreacted dye was removed by gel filtration chromatography on a HiPrep 26/10 desalting column run on an FPLC AKTA Purifier system (GE Healthcare, GB), followed by at least five consecutive centrifugations using a Microcon YM-10 concentrator, until the solution coming through the concentrator did not contain any dye, as assayed by absorbance spectroscopy. LysoUB was synthesized by covalently attaching the UniBlue A probe to the primary amino group of the lysoPE headgroup as previously described (*18*). Large unilamellar vesicles (LUV) of 0.1 μm diameter were prepared by extrusion (*19*, *20*) using the following molar mixtures of POPC and POPG: 1-to-3 (25PC:75PG), 3-to-1 (75PC:25PG), and 9-to-1 (90PC:10PG). Lipid concentrations of stock solutions were determined according to the procedure of Bartlett (*21*).

Preparation of Single-Cys Mutants (N235C, L350C, Q369C, and P378C). pET15b plasmid containing the diphtheria toxin T-domain gene with mutation C201S has been used as template for mutagenesis. Introduction of point Cys mutations for specific labeling with corresponding dye derivatives was performed by site-directed mutagenesis with the QuikChange site-directed mutagenesis kit from Stratagene (Cedar Creek, TX) and verified by DNA sequencing with T7 primer. Protein expression was performed in BL21 DE3pLys *Escherichia coli* cells, and recombinant protein synthesis was induced by addition of 0.8 mM IPTG at $OD_{600} = 0.5$, after which cells were grown at 25 °C overnight. Purification included affinity chromatography on Ni-NTA resin from Qiagen (Valencia, CA) and gel filtration on a Sepharose 12 1×30 cm column from GE Healthcare (Giles, U.K.) in PBS buffer containing 0.1 mM EDTA. The purity of preparations obtained was analyzed by SDS−PAGE. For determination of protein concentrations we used a molar extinction coefficient of 17000 M^{-1} cm^{-1} at 278 nm.

Kinetic Measurements of Membrane Binding and Insertion. T-domain binding and insertion kinetics were measured using FRET and NBD fluorescence signals, respectively. LUV binding was assayed by energy transfer from the Alexa488-labeled N235C mutant to LUV containing a 1−2% molar fraction of Rhodamine-PE. Normally, 0.2 μM labeled T-domain was mixed with 1 mM LUV in 50 mM phosphate buffer at pH 8, and membrane binding and insertion were initiated by manual injection of the appropriate aliquots of the 0.5 M acetic buffer. Fluorescence was measured using a SPEX Fluorolog FL3-22 steady-state fluorescence spectrometer (Jobin Yvon, Edison, NJ) equipped with double-grating excitation and emission monochromators. The measurements were made in a 2×10 mm cuvette oriented perpendicular to the excitation beam and maintained at 25 °C using a Peltier device from Quantum Northwest (Spokane, WA). For NBD measurements excitation and emission wavelengths were 465 and 530 nm, respectively, and the slits were 2 nm. For FRET measurements excitation and emission wavelengths were 455 and 515 nm, respectively, and the slits were 5 nm. In both types of measurement the data were collected with a 10 s interval. For the purpose of presentation, FRET kinetic data, which show a stepwise *decrease* in donor signal upon association of LUV and T-domain, were renormalized to show a corresponding stepwise *increase* in binding. This algebraic transformation consisted of the following steps: (a) dividing the signal at pH 8 by the kinetic curve, (b) subtracting this ratio from 1, and (c) normalizing all of the data to the maximal level of binding of a 100% (which is confirmed by FCS).

Kinetics of the formation of the transmembrane-inserted T-state of the DTT were fitted to the following empirical three-component exponential association equation:

$$F_T(t) = A_0 + A_1(1 - e^{-k_1 t}) + A_2(1 - e^{-k_2 t}) \quad (1)$$

where A_i are the amplitudes of the corresponding kinetic component with apparent rates of k_i (A_0 corresponds to an

infinitely fast component with $k_0 = 0$). For single-component and double-component fits, additional amplitudes were assumed zero, $A_0 = A_2 = 0$ and $A_0 = 0$, respectively. The sum of all amplitudes corresponds to the total fraction of insertion-competent state (i.e., fraction of protein that can insert under given conditions after infinite time): $F_{IC} = A_0 + A_1 + A_2$.

Time-Resolved Fluorescence Measurements of Membrane Topology Analysis. Fluorescence decays were measured with a time-resolved fluorescence spectrometer, FluoTime 200 (PicoQuant, Berlin, Germany), using a standard time-correlated single-photon counting scheme as previously described (*22*). Samples were excited at 439 nm by a subnanosecond pulsed diode laser, LDH 440 (PicoQuant, Berlin, Germany), with a repetition rate of 10 MHz. Fluorescence emission was detected at 536 nm, selected by a Sciencetech Model 9030 monochromator, using a PMA-182 photomultiplier (PicoQuant, Berlin, Germany). The samples normally contained 0.4 μM protein and 1−2 mM lipid. LysoUB from micellar suspension in buffer was added after 2 h of incubation of protein and LUV. The fluorescence intensity decay was analyzed using FluoFit iterative-fitting software based on the Marquardt algorithm (PicoQuant, Berlin, Germany).

FCS Measurements. The details of FCS measurements and analysis were the same as previously described (*16*). All samples contained a large excess of LUV (1−2 mM) over T-domain (1 nM). The experiment was conducted on a MicroTime 200 confocal microscope (PicoQuant, Berlin, Germany). The fluorescence was excited with a pulsed picosecond diode laser, LDH-P-C-470, operated at 40 MHz. The fluorescence was detected confocally after passing through an emission bandpass filter, AHF/Chroma: HQ 520/40 blocking the excitation wavelength. In order to suppress influences from the afterpulsing typically observed with single photon avalanche diodes (SPAD), the fluorescence light was split with a 50/50 beam splitter cube onto two SPADs (SPCM-AQR-14; Perkin-Elmer Inc.), and cross-correlation analysis was applied. The high numerical aperture apochromatic water immersion objective (60×, NA 1.2; Olympus), together with the 50 μm confocal pinhole, resulted in a confocal detection volume of 1 fL. The fluorescence was detected applying time-correlated single photon counting (TCSPC) with the TimeHarp 200 board. The data were stored in the time-tagged time-resolved mode (TTTR), which allowed the recording of every detected photon with its individual timing and detection channel information.

FCS Data Analysis. The autocorrelation function for single diffusing species undergoing Brownian motion can be described with the equation (*23*, *24*):

$$G(\tau) = \frac{1}{N} g(\tau)$$

$$= \frac{1}{N}\left(1 + \frac{T}{1-T} e^{-\tau/\tau_{Tr}}\right)\left(\frac{1}{1+\tau/\tau_D}\right)\left(\frac{1}{1+\tau/S^2\tau_D}\right)^{1/2} \quad (2)$$

where N is the average number of fluorescent molecules in the focus volume and τ_D is the correlation time of the particles. The correlation time represents the diffusion time through the focus volume and equals $\tau_D = \omega^2/4D$, where ω^2 is the square of the radius of the laser focus and D is the diffusion constant. S is the ratio of the distances from the center of the laser beam focus in the radial and axial directions, respectively. T is the fraction of fluorophores in the triplet state and τ_{Tr} is the triplet lifetime (~2 μs in our case).

The measured correlation function $G(\tau)$ of a multicomponent system is a weighted sum of the autocorrelation functions of each component $G_i(\tau)$ with amplitudes A_i (*24*−*26*) as

$$G(\tau) = \sum_{i=1}^{M} q_i^2 N_i^2 G_i(\tau) \Big/ \left(\sum_{i=1}^{M} q_i N_i\right)^2$$

$$= \sum_{i=1}^{M} q_i^2 N_i g_i(\tau) \Big/ \left(\sum_{i=1}^{M} q_i N_i\right)^2 = \sum_{i=1}^{M} A_i g_i(\tau) \quad (3)$$

where N_i is the mean particle number and q_i is the ratio of the fluorescence yield of the ith component to that of the first component. In our system $q_i = 1$, as binding of the dye-labeled T-domain to vesicles does not change the fluorescence intensity of Alexa488. For our system the following two diffusing species were considered: the fluorescently labeled proteins (index P) and LUV with bound fluorescently labeled proteins (index V):

$$G(\tau) = A_P g_P(\tau) + A_V g_V(\tau) \quad (4)$$

FCS Data Analysis. Information on the fraction of free and bound protein can be extracted from the values of weighting factors A_P and A_V (*16*, *24*). Here we worked under conditions of a so-called "infinite dilution regime" which is achieved because of an overwhelming molar excess of lipid over protein (~10^6). Under such conditions each vesicle contains no more than a single protein, and therefore, the number of particles associated with the slow mobility is equal to the number of vesicle-bound proteins. This substantially simplifies calculation of the fraction of bound protein (*26*), which under conditions of lipid saturation is equal to the fraction of the membrane-competent form F_{MC} (*16*):

$$F_{MC} = \frac{A_V}{A_V + A_P} \quad (5)$$

The pH dependencies of the fraction of the membrane-competent form constituting binding titration profiles were fitted to the equation:

$$F_{MC} = \frac{1}{1 + 10^{n(pH - pK_a)}} \quad (6)$$

where pK_a is a negative logarithm of the dissociation constant and n is the Hill coefficient. The same equation is also utilized to fit the pH dependence of the fraction of the insertion-competent state F_{IC}.

RESULTS

FCS Experiments at Lipid Saturation. First, we determine the pH dependence of the formation of a membrane-competent form of the protein using fluorescence correlation spectroscopy (FCS). We have used this technique to study pH-dependent membrane interactions of ANX (*16*). While lipid titration at constant pH allows measurements of the free energy of membrane association (*27*), measurements of vesicle-associated protein at *lipid-saturating* conditions yield the fraction of membrane-competent protein F_{MC}. For FCS measurements, a single-cysteine N235C mutant of the T-domain was labeled with Alexa488. The probe was attached at the exposed residue at the N-terminal segment not expected to insert into the lipid bilayer. A typical example of the normalized autocorrelation data collected in such an

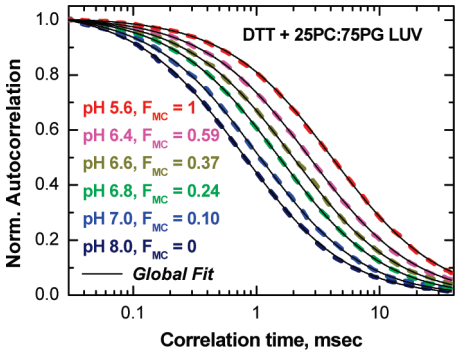

FIGURE 2: Example of the binding measurement using FCS performed under conditions of the "infinite dilution regime" satisfied at an extremely high lipid excess over fluorescently labeled protein (see text). Acidification results in a progressive shift of mobility from that of the free T-domain to that of a vesicle-bound T-domain. Quantitative determination of the membrane-competent fraction, F_{MC}, is achieved by a linked analysis (solid lines) of fluorescence autocorrelation curves (dashed lines) that links the two correlation times for all curves and allows free fitting of the preexponential amplitudes (see eqs 2−4 and ref *16*). For the purpose of better visual representation all data are normalized to the same number of fluorescent particles in the focal volume. Note that the absolute values of amplitudes are not important under these conditions, just their relative contributions (eq 5).

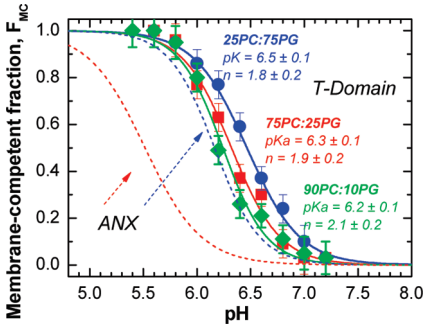

FIGURE 3: pH dependences of FCS-measured formation of the membrane-competent form of the diphtheria toxin T-domain (symbols and lines) and ANX (*16*) (only fitting curves are shown for ANX). Titration profiles of the T-domain are shifted toward neutral pH and are less dependent on the lipid composition of the vesicles: 25PC:75PG, 75PC:25PG, and 90PC:10PG are shown in blue, red, and green respectively. The data were fitted to eq 6 to determine the apparent pK_a and n values presented on the graph. Experimental details are the same as in ref *16*.

experiment for samples containing 1 nM labeled T-domain and 1 mM LUV at various pH is shown in Figure 2. The observed pH-dependent shift reflects the increase in membrane-associated T-domain. A lower mobility of a relatively large vesicle (~100 nm diameter) compared to a free protein molecule is sufficient to make single color autocorrelation measurements useful for binding studies. The advantage of FCS measurements is that their great sensitivity allows one to work in an infinite dilution regime which simplifies mathematical treatment of the system (see Materials and Methods and discussion in ref *16*). Because no changes in relative fractions of the bound and free T-domain were observed when the concentration of vesicles was increased or decreased 2-fold (not shown), we conclude that we do indeed work under lipid-saturating conditions and membrane-bound fractions correspond to membrane-competent fractions F_{MC} of the T-domain at a given pH (see Figure 8 and Discussion).

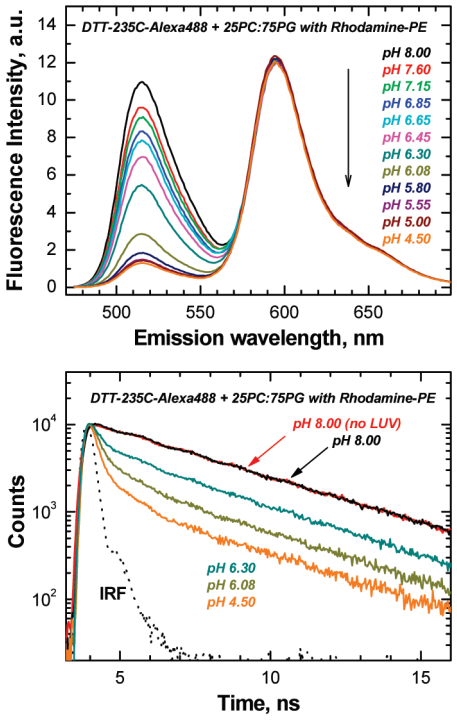

FIGURE 4: Example of the binding measurement using FRET between the donor-labeled T-domain and acceptor-labeled lipid vesicles (see text). Lowering the pH results in membrane association which can be detected by the reduction of the intensity of the donor emission (A) and shortening of the donor excitation lifetime (B).

The plots of F_{MC} vs pH, referred to as titration profiles of membrane binding, contain information on the protein protonation required for membrane association (Figure 3). Our results reveal two important differences between the T-domain and ANX protonation studied earlier (*16*). First, formation of the membrane-competent T-domain occurs in a higher pH range, and second, it exhibits only a mild dependence on the lipid composition. In general, the following two limiting cases should be considered for interpreting pH-triggered membrane association: (a) protonation occurs predominantly in the bulk phase of solution and (b) protonation occurs predominantly on the interface. The first scenario will result in titration profiles being completely independent of the lipid bilayer, while in the second one a relatively strong dependence on the surface potential is expected. Protonation of ANX falls under the latter case, exhibiting strong variation depending on the concentration of anionic lipids (red and blue dotted lines correspond to 75PC:25PG and 25PC:75PG, respectively). This difference can be quantitatively explained by the variation in local concentrations of protons near the membrane interface (*16*). Clearly, the T-domain does not share the strong lipid dependence of titration profiles of ANX (Figure 3), indicating the importance of solution protonation as compared to interfacial protonation.

Equilibrium and Kinetic FRET Binding Experiments. While FCS measurements provide a very sensitive tool to study formation of the membrane-competent form under equilibrium conditions, they are not readily applicable to kinetic measurements. To study time-dependent association with the membrane, we used kinetic measurements of the FRET signal between the donor-labeled T-domain and acceptor-labeled LUV. First, we checked the validity of this FRET approach by measuring equilibrium titration profiles and comparing them to those obtained by FCS. We have used the same T-domain samples

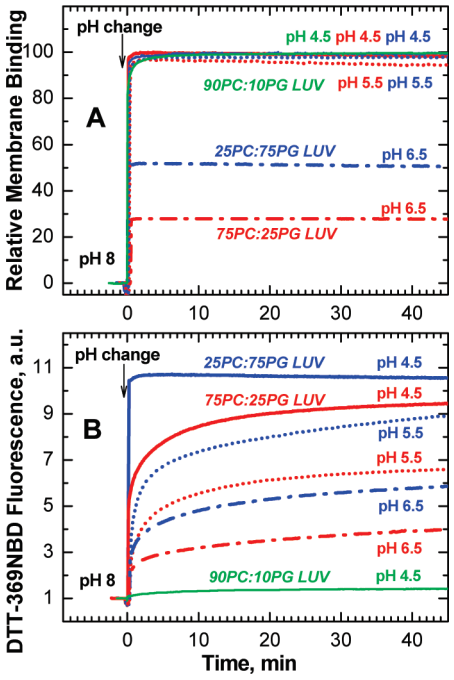

FIGURE 5: Membrane binding and insertion kinetics of the T-domain measured with LUV of specified lipid compositions (color coded) at various pHs (line coded). (A) Binding kinetics were followed by the change in FRET signal between the donor-labeled T-domain and acceptor-labeled LUV. (B) Insertion kinetics were followed by changes in fluorescence intensity of the environment-sensitive probe NBD attached to the center region of the membrane-insertion domain (Q369C-NBD). Membrane interactions were triggered at zero time by lowering the pH of the sample from pH 8 (no interaction; see Figure 3) to the desired final value. Differences observed in the two types of kinetics reveal the insertion intermediate, which depends on pH and lipid composition.

as for FCS with an Alexa488 fluorophore attached at position 235 but have added a 2% acceptor-labeled lipid (Rhodamine-POPE) to lipid vesicles. Typically, samples containing 0.2 μM labeled protein and 2 mM lipid LUV were placed at buffers of different pH, and their steady-state and time-resolved fluorescence properties were measured (Figure 4). Change in pH from neutral to acidic resulted in changes of donor emission intensity (Figure 4A) and shortening of the excited state lifetime of the donor (Figure 4B). The acceptor peak of emission did not undergo a substantial change, because it was mainly due to direct excitation (note a 100-fold excess of acceptor over donor). The titration curves generated from the reduction in donor emission were in good agreement with FCS results in Figure 3, and the variation of pK_a determined by FCS and FRET did not exceed 0.1 (not shown).

The advantage of FRET measurements over FCS, however, is the relatively fast data acquisition, which allows kinetic measurements of membrane association. We have measured the changes in donor emission upon mixing the T-domain at different pHs with acceptor-labeled vesicles composed of the three lipid compositions used before. Since we have determined the range of changes corresponding to complete binding, we could easily convert these time-dependent intensity changes into binding kinetics by a simple algebraic transformation, described in the Materials and Methods section. Our results presented in Figure 5A indicate that membrane association of the T-domain occurs relatively quickly (< 1 min) regardless of the pH or lipid composition and even under conditions of incomplete binding (curves at pH 6.5). While it is possible that lipid composition and pH do affect the rate of binding, experimental exploration of their effect will require stopped-flow measurements. This does not affect, however, the conclusions of this study nor the interpretation of insertion steps presented below, as those occur on a much slower time scale.

Equilibrium and Kinetic Insertion Experiments. We have compared FRET-based binding kinetics in Figure 5A to those observed with the environmentally sensitive probe NBD attached to a single-Cys residue in the Q369C mutant of the T-domain. Previous EPR experiments (*6*) showed that a spin label attached to this residue is relatively exposed in the soluble T-domain at neutral pH (W-state) and is placed roughly in the middle of the bilayer in the final TM conformation at low pH (T-state). Such a transition is expected to result in a substantial increase of the fluorescence of NBD, which is indeed observed. The advantage of fluorescence measurements over the EPR is that the kinetics of the transition is easily measured (Figure 5B). In contrast to the fast FRET-based binding kinetics, fluorescence kinetics of NBD are slow, indicating the existence of a membrane-bound, but not fully inserted, intermediate (I-state). Remarkably, the insertion kinetics demonstrate that I-to-T transition is already occurring at pH 6.5, at which point the binding W-to-I transition is only half-completed (dashed-dotted lines in Figure 5A). This means that the protonation transitions allowing membrane binding and TM insertion are staggered, which could be related to an additional protonation of the T-domain on the interface due to variation in pK_a in bulk of solvent and the membrane interfacial zone (see Discussion).

The exact time dependencies of intensities are complex and nonexponential and will be quantitatively analyzed in a subsequent section. Nevertheless, it is clear that both the rate and the final degree of intensity change are dependent on pH and lipid composition, with anionic lipids promoting the insertion. The most striking result is the virtual absence of the insertion-associated signal observed with vesicles of low anionic lipid content (90PC:10PG, Figure 5B, green line), for which rapid and complete binding is observed in a FRET kinetics (Figure 5A, green curve). This leads to the suggestion that the noninserted intermediate is stabilized by this lipid composition, which can be verified using our fluorescence lifetime quenching topology method (*22*), which we have also used for studies of ANX insertion (*16*).

To test the insertion topology, we attached the NBD probe to the very tip of the insertion domain formed by helices TH8 and TH9 using the L350C mutant (Figure 1). If these helices adopt the TM conformation upon insertion, the probe will be translocated across the bilayer and become inaccessible to the externally added LysoUB quencher. If the helices remain interfacial, the quenching will be substantial. We have performed LysoUB quenching experiments after T-domain insertion has come to equilibrium at 1 h after mixing the T-domain and LUV at low pH. In order to describe LysoUB quenching, and the resulting topology, in a quantitative way, we have analyzed the fluorescence decay for all samples and calculated the ratio of the average lifetime upon addition of the quencher (Table 1), as described previously (*22*). Comparison of the quenching in well-defined model systems indicates that the ratio of the longest decay time in the absence (τ_0) and presence of 2% LysoUB (τ) is sensitive to the topology of the NBD-labeled site: (a) weak quenching ($\tau_0/\tau \leq 1.25$) indicates translocation to the *trans* side of the bilayer; (b) strong quenching ($\tau_0/\tau \geq 1.45$) indicates lack of translocation (*22*).

Table 1: Experimental Determination of *cis* or *trans* Topology of Several NBD-Labeled Mutants Using Fluorescence Lifetime Quenching with LysoUB[a]

T-domain labeling site	LUV	LysoUB	τ_1, ns (α_1)	τ_2, ns (α_2)	τ_α, ns	τ_α/τ_0 (topology)
350C-NBD	25PC:75PG	none	1.50 (0.32)	7.90 (0.68)	5.85	1.12 (*trans*)
		+2%	1.42 (0.37)	7.47 (0.63)	5.25	
350C-NBD	75PC:25PG	none	1.33 (0.35)	7.20 (0.65)	5.13	1.11 (*trans*)
		+2%	1.32 (0.40)	6.79 (0.60)	4.61	
350C-NBD	90PC:10PG	none	1.18 (0.50)	6.27 (0.50)	3.72	1.70 (*cis*)
		+2%	0.94 (0.59)	3.97 (0.41)	2.19	
378C-NBD	25PC:75PG	none	1.23 (0.51)	4.54 (0.49)	2.98	1.72 (*cis*)
		+2%	0.85 (0.67)	3.50 (0.33)	1.73	

[a] See ref *22*. τ_i and α_i are individual lifetime components; τ_α and τ_0 are amplitude-averaged lifetimes in the presence and in the absence of LysoUB quencher. *cis* and *trans* topologies are assigned based on the value of the τ_α/τ_0 ratio based on the hallmarks established in a model study (*22*).

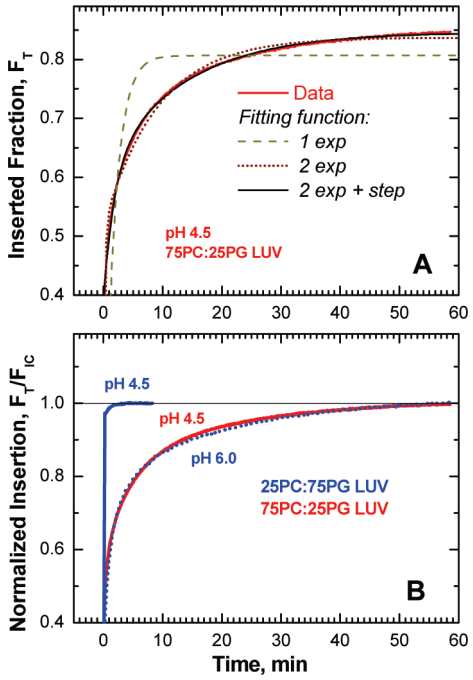

FIGURE 6: Quantitative analysis of insertion kinetics. (A) Comparison of fitting with various exponential association models (eq 1 and text for details) of the time-dependent insertion of DTT-369-NBD into the 75PC:25PG lipid bilayer at pH 4.5 (solid red line). The following parameters correspond to three fitting curves: single exponential $A_1 = 0.81$, $k_1 = 9.4 \times 10^{-3}$ s^{-1} (dashed line); double exponential $A_1 = 0.52$, $k_1 = 8.3 \times 10^{-2}$ s^{-1}, $A_1 = 0.32$, $k_1 = 1.8 \times 10^{-3}$ s^{-1} (dotted line); double exponential with a step $A_0 = 0.42$, $A_1 = 0.22$, $k_1 = 0.9 \times 10^{-2}$ s^{-1}, $A_1 = 0.23$, $k_1 = 1.2 \times 10^{-3}$ s^{-1} (solid black line). While the latter two models produce a similar fit, the monoexponential function does not adequately describe the kinetics, indicating the existence of a distinct intermediate insertion-competent state. Kinetic parameters for other lipid compositions and pH values are summarized in Table 2. (B) Comparison of the time-dependent changes in T-domain insertion into two lipid systems: 25PC:75PG (blue) and 75PC:25PG (red). For visual comparison the fractions of protein in the inserted T-state, F_T, are normalized to its final value (fraction of insertion-competent state, F_{IC}) for each sample.

Consistent with the expectations from kinetic data we found that the degree of quenching depends on the lipid composition. The lifetime ratio of about 1.1 observed in 75PC:25PG and 25PC:75PG is indicative of efficient translocation, while the ratio of 1.7 observed in 90PC:10PG confirms interfacial topology. In fact, the same quenching ratio was observed in a control experiment using the NBD-labeled P378C mutant (Table 1), for which no translocation is expected during TH8−TH9 insertion (Figure 1).

Table 2: Quantitative Analysis of Insertion Kinetics Using Eq 1[a]

lipid	pH	A_0	A_1	k_1 (s^{-1})	A_2	k_2 (s^{-1})	F_{IC} ($= A_0 + A_1 + A_2$)
25PC:75PG	6.5	0.17	0.13	0.7×10^{-2}	0.13	0.7×10^{-3}	0.51
	6.0	0.19	0.36	1.8×10^{-2}	0.21	1.1×10^{-3}	0.76
	5.5	0.20	0.36	1.4×10^{-2}	0.34	0.5×10^{-3}	0.90
	4.5	0.96	0.04	1.8×10^{-2}	0.00		1.00
75PG:25PG	6.5	0.07	0.06	1.0×10^{-2}	0.13	0.5×10^{-3}	0.26
	5.5	0.11	0.23	1.3×10^{-2}	0.24	1.2×10^{-3}	0.58
	4.5	0.42	0.22	0.9×10^{-2}	0.23	1.2×10^{-3}	0.87

[a] See text for details.

Quantitative Analysis of Insertion Kinetics. We have analyzed the insertion kinetics as described in the Materials and Methods section (eq 1) and found them to be nonexponential. The example of application of various fitting functions to the data generated for the 75PC:25PG pH 4.5 sample and normalized to relative signal change between the noninserted and completely inserted sample is presented in Figure 6A. The monoexponential association equation operating with just two fitting parameters produces an obviously poor result (dashed line), with a low correlation parameter ($R^2 = 0.56$) and high reduced chi-squared ($\chi^2 = 2.6 \times 10^{-3}$). The double-exponential model which utilizes four fitting parameters fits much better (dotted line, $R^2 = 0.98$, $\chi^2 = 10^{-4}$), though it also exhibits some nonrandom deviations from the data. The best fit is archived by a five-parameter function (solid black line, $R^2 = 0.99$, $\chi^2 = 10^{-5}$) in which two-component association is combined with a step at zero time, which is an equivalent of a third kinetic component with a correlation time much faster than the mixing dead time of 10 s. This component, however, should not be confused with the binding transition from water-soluble to interfacial state which also occurs more quickly than the detection limit of the hand-mixing experiment, as the amplitude of this component is much larger than the amplitude associated with transition to the interfacial state. The second and third components have rates in the range of $0.7-1.8 \times 10^{-2}$ s^{-1} and $0.7-1.2 \times 10^{-3}$ s^{-1}, respectively (Figure 6A and Table 2). A peculiar observation on the interplay of the effects of pH and lipid composition on insertion rates is illustrated in Figure 6B. The three insertion kinetics are normalized to the final insertion level to allow a better visual comparison of the time-dependent change. Decrease of anionic lipid content from 75% to 25% at pH 4.5 leads to substantial slowing of the insertion (compare solid blue and red lines). Interestingly, lowering the pH from 4.5 to 6.0 for the 25PC:75PG LUV (blue dashed line) results in a very similar kinetic effect.

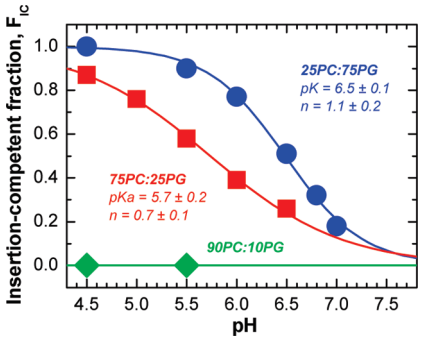

FIGURE 7: pH-dependent formation of the insertion-competent state of the T-domain (see text for details). Insertion is promoted by anionic lipids (75PC:25PG, red; 25PC:75PG, blue), and no insertion is observed in 90PC:10PG membrane (green), which is confirmed by topology experiments (Table 1). The formation of the insertion-competent state is a result of a pH-dependent transition, distinct from the one resulting in the formation of the membrane-competent state (compare to titration profiles in Figure 3).

Fitting insertion kinetics not only is useful for the determination of rates but also helps with more accurate estimates of the equilibrium insertion levels. We have used the sum of all of the amplitudes A_i to determine the pH dependence of final insertion fraction for all three lipid compositions (Figure 7). The insertion titration profile for 25PC:75PG LUV (blue circles) is similar to the binding titration profile for this lipid (Figure 7, blue circles), indicating that eventually all bound protein will be inserted. This is not the case for lipid compositions with a smaller fraction of anionic lipids. For 75PC:25PG the pH-dependent insertion profile is much shallower and shifted toward acidic pH (red squares), while for 90PC:10PG it is totally blocked (green diamonds). The latter is confirmed by LysoUB topology measurements (Table 1). The difference in lipid dependencies of binding and insertion transitions (compare corresponding curves in Figures 3 and 7) indicates that these are two different, but staggered, pH-dependent transitions (see Discussion).

DISCUSSION

pH-Dependent Formation of the Membrane-Competent Form. The initial step in pH-triggered membrane insertion of the T-domain is the formation of a membrane-competent form, suggested to have properties similar to that of a molten globule state (*12*). Previously, we have used FCS measurements to characterize the formation of the membrane-competent state for another protein capable of undergoing acid-induced TM insertion, annexin B12 (ANX) (*16*). Application of the same FCS methodology (confirmed by independent FRET-based binding assay) to the T-domain indicates that the protonation leading to the formation of the membrane-competent form shows modest effect on lipid composition and hence on the surface potential, φ. The apparent pK_a values of titration profiles measured with 90PC:10PG ($\varphi = -28$ mV), 75PC:25PG ($\varphi = -72$ mV), and 25PC:75PG ($\varphi = -103$ mV) LUV differ only slightly, indicating that protonation in bulk solution plays a major role. The difference in pK_a for 75PC:25PG and 25PC:75PG observed for ANX is 4-fold higher than that for the T-domain, which can be explained by interface-induced protonation of ANX and local variation of pH near the bilayer surfaces with different anionic lipid content. Once this variation is accounted for, the corrected lipid-independent pK_a value for ANX can be obtained, which equals pK_a = 4.3 (*16*). This is two pH units lower than that observed with the T-domain (Figure 3), which could be related to the difference in the nature of titratable residues in the two proteins. It has been suggested before that histidine protonation is important for the action of the T-domain (*13*, *28*), which is consistent with the relatively high pK_a of 6.2−6.5 observed for the formation of the membrane-competent T-domain (Figure 3).

While anionic lipids do not cause a substantial shift in protonation, they are nevertheless required for proper membrane binding of the T-domain. We have noticed that using pure POPC LUV or even reducing POPG content to 5% leads to protein aggregation and lack of reproducible membrane binding. Clearly, the initial role of anionic lipids (at least *in vitro*) is to capture the T-domain to the membrane and prevent its aggregation and precipitation at pH values below 6.

Topology of the TH8−9 Helical Hairpin in the Final Inserted State. The exact topology of the insertion hairpin, consisting of helices TH8 and TH9, has been suggested to depend on the exact nature of the sample. The EPR measurements that indicate a TM conformation of these helices (*6*) are performed using LUV as a membrane system and using a lipid-to-protein ratio of $R_i = 500$. Normally, the inserted T-domain is separated from the rest of the sample by centrifugation prior to EPR measurements. On the other hand, according to the published fluorescence results, efficient formation of the "deep" TM form of the T-domain requires either a high protein concentration (or low $R_i \sim 400$) or the use of short-chained lipids, such as dimyristoleoylphosphatidylcholine (*10*) and can proceed only in small unilamellar vesicles, SUV (*10*), but not in LUV (*11*). (Unlike larger extruded LUV, sonicated SUV are not equilibrium structures and can result in irregular protein and peptide penetration as discussed in ref *29*.) To confirm that, in our LUV system, the T-domain does indeed adopt a TM conformation, we have applied our recently developed fluorescence lifetime quenching topology method (*22*). The obtained quenching results (Table 1), in combination with the kinetic results shown in Figure 5B, demonstrate that TM insertion occurs in LUV formed of regular length lipids such as POPC and POPG mixtures even at a high lipid-to-protein ratio of 3000−5000.

Kinetic Insertion Intermediate. Over the years several research groups have presented compelling evidence for the T-domain adapting multiple conformations on the membrane (*10*−*13*, *15*); however, the kinetics of the transition between those forms has never been addressed. Several of those studies used intrinsic tryptophan fluorescence as a primary tool, which makes kinetic measurements difficult to implement and interpret due to low signal-to-noise ratio and sometimes redundant spectroscopic response of tryptophan emission to binding, refolding, and insertion. Here, by applying several specific spectroscopic approaches, we were able to separate kinetics of binding (Figure 5A) and insertion (Figure 5B) and explicitly demonstrate the existence of the interfacial insertion intermediate. Direct observation of an interfacially refolded kinetic intermediate in the T-domain insertion pathway confirms the importance of understanding the various physicochemical phenomena (e.g., interfacial protonation (*30*), nonadditivity of hydrophobic and electrostatic interactions (*31*, *32*), and partitioning−folding coupling (*33*, *34*)) that occur on membrane interfaces.

The insertion intermediate can be stabilized in its interfacial location by the use of a low 10% content of anionic lipids. This again distinguishes the T-domain from ANX, in which the interfacial intermediate is trapped on bilayers with a high anionic lipid content (*16*, *18*). The latter can be explained by the

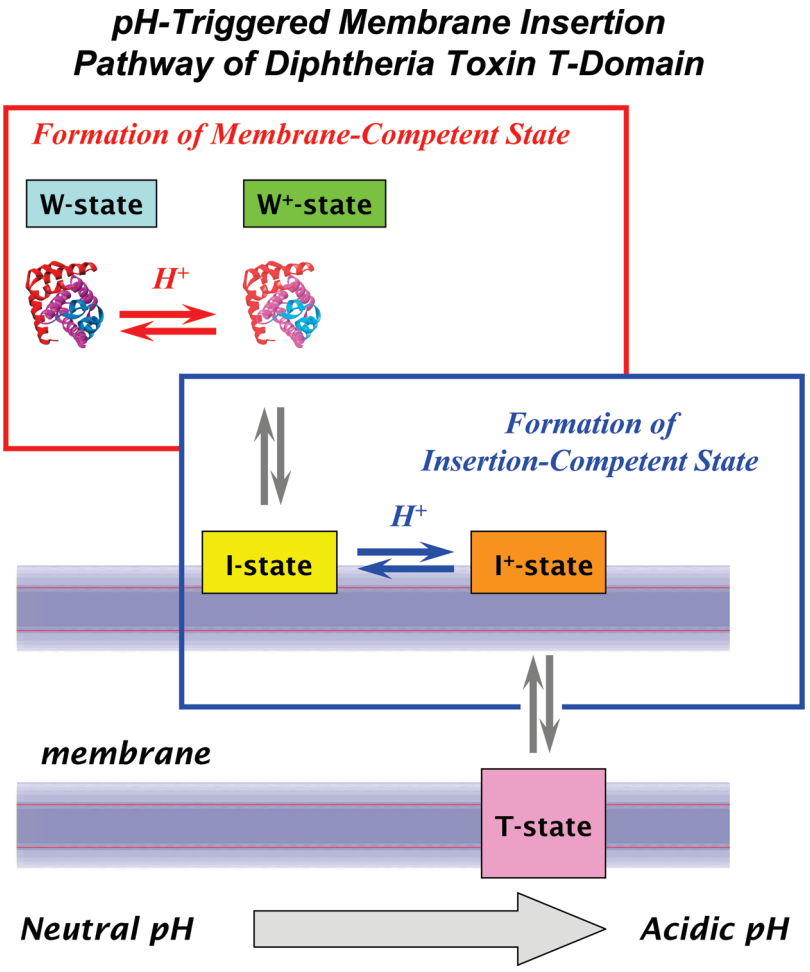

FIGURE 8: Schematic representation of the pH-dependent membrane insertion pathway of the diphtheria toxin T-domain. Initial protonation, resulting in the formation of the membrane-competent W^+-state, occurs primarily in the bulk of solution and depends little on the properties of the bilayer (Figure 3). In the presence of membranes this state rapidly associates with the bilayer to form an interfacial intermediate I-state (Figure 5A). Subsequent insertion is facilitated by the presence of anionic lipids (Figure 5B, Table 2), which promote the formation of the insertion-competent I^+-state (Figure 7) and decrease the thermodynamic barrier for insertion into the T-state (Figure 6B). The two protonation steps responsible for the formation of conformations capable of membrane association (W-to-W^+ transition, red rectangle) and insertion (I-to-I^+ transition, blue rectangle) have overlapping pH ranges, suggesting that additional protonation can occur at the same pH value due to the shift of pK_a values of titratable residues after their partitioning into the interfacial zone of the lipid bilayer (see text).

stabilizing Coulombic interactions between anionic lipids and cationic residues present in the translocating segments of the ANX. In contrast, in the T-domain, the only cationic residues in the TH8−TH9 segment are located in the top part of the helical hairpin (H322, H323, H372, and R377) and thus will not prevent its insertion. As a matter of fact, placing a pair of charges on the top of each helix may assist insertion by destabilizing the soluble fold by interaction with anionic lipids. Possibly, lipid interaction with these residues results in the formation of the insertion-competent state and explains the observed promotion of the insertion by anionic lipids (Figures 5−7).

The intermediate, trapped on the bilayer interface in the 90PC:10PG membrane (I-state in Figure 8) has a distinct spectroscopic signature, which sets it apart from the inserted form (T-state) populated in other lipid compositions. For example, the emission spectra of NBD attached in positions 350 and 369 exhibit a 4−5 nm red spectral shift in I-state, compared to T-state (not shown). Also, transition from W-state to I-state results in a red shift of the position of intrinsic tryptophan fluorescence (from 339 to 345 nm), indicating a certain degree of unfolding and exposure of W206 and W281 into aqueous environment. The position of maximum of the T-state is blue shifted (335 nm), consistent with increased hydrophobicity of tryptophans' environment due to insertion.

The Insertion-Competent State. Previously, we have analyzed kinetic insertion of the ANX along the pathway leading from aqueous W-state to transbilayer inserted T-state via an interfacial intermediate I-state (*16*, *18*). For the T-domain, however, this simple W-to-I-to-T scheme needs to be modified. The nonexponential kinetics of insertion transition (Figure 6A) clearly indicates the existence of at least a single intermediate populated after the initial binding event (formation of I-state) but before the final insertion is achieved (formation of T-state). Similarly to the membrane-competent state, we refer to this intermediate as an insertion-competent state. While the formation of the *membrane-competent* state (or membrane binding-competent state) leads to the conformation that can bind membrane, the formation of the *insertion-competent* state leads to the state that can adopt a TM conformation. The formation of this intermediate is both lipid- and pH-dependent with anionic lipids being essential for its formation (i.e., increasing the population of protein capable of insertion at a given pH, Figure 7), as well as for increasing the overall insertion rate (Figure 6B). The mechanism for these effects is not known,

though one can reasonably assume that variation in the local concentration of protons near membranes with different contents of anionic lipids can play a certain role. This effect can lead to an up to 0.6 pH unit difference in local pH near membranes containing 25PC:75PG and 75PG:25PC (*16*). This is not sufficient, however, to explain the 1.5 unit pH shift between samples of different lipid compositions but similar kinetic rates (Figure 6B), and other explanations involving direct interaction of anionic lipids with the intermediate and insertion-activated transient state should be considered.

For a general reaction containing a single intermediate (A ↔ B ↔ C), the formation of the final state follows a biexponential law, in which the apparent kinetic parameters are complex functions of the four kinetic rates for each of the direct and reverse reaction steps (*35*). The assumption that under the conditions of the experiment the reverse reactions can be neglected simplifies the mathematical expressions and results in the apparent kinetic rates coinciding with the two rates for each step of the direct reaction (*18*). Our data indicate that in general a three-component exponential association function is needed to fit the data (Figure 6A, Table 2), although a two-component function produces a close fit. This could be an indication that more than one intermediate exists on the pathway from I-state to T-state or that conformational heterogeneity of the T-domain leads to multiple pathways. In each case, the slowest observed rate ($\sim 10^{-3}$ s^{-1}) will correspond to the formation of the rate-limiting intermediate, which we call insertion-competent state (I^+-state, Figure 8). The final insertion (I^+-to-T transition) is much faster, and the determination of its exact rate is complicated by the resolution of the hand-mixing technique used in this study. In future studies we will further address the details of the T-domain insertion pathway by using stopped-flow mixing as well as designing a spectroscopic experiment which will selectively identify various folding/insertion intermediates (e.g., by using a double kinetic approach (*36*)).

Insertion Pathway with Two Staggered pH-Dependent Transitions. Various aspects of the pH-triggered bilayer insertion of the T-domain are illustrated using a pathway scheme in Figure 8. The initial protonation step, the formation of the membrane-competent form W^+, occurs in solution and depends little on the properties of the membrane as long as a certain minimal amount of anionic lipids is present. The T-domain in this membrane-competent conformation is susceptible to aggregation, but it can be stabilized by fluorinated nondetergent surfactants that act as insertion chaperones (*14*, *37*). Application of such surfactants is essential for equilibrium thermodynamic studies of insertion (*27*) but is not practical for kinetic studies. In the presence of membranes the W^+-state rapidly associates with the bilayer interface (I-state). It is not clear what structural rearrangements are associated with this transition. Final TM insertion requires the formation of the insertion-competent form (I^+), which is populated in another pH-dependent transition. Unlike the W-to-W^+ transition (Figure 3), this I-to-I^+ transition depends strongly on the presence of anionic lipids (Figure 7). This transition is totally suppressed in 90PC:10PG LUV and broadened in 75PC:25PG LUV, as compared to 25PC:75PG LUV. The observed broadening can be a manifestation of a combination of two transitions being spread along the pH coordinate for the T-domain in the 75PC:25PG bilayer. It is also possible that insertion of other parts of the protein plays a role in the insertion of the TH8−TH9 segment (possibilities of cooperativity in insertion transitions are described here (*38*)). It has been suggested that a concerted His protonation is important for membrane interaction of the T-domain (*28*) and that protonation of E349 and D352 at the tip of the TH8−TH9 hairpin is responsible for translocation (*39*). Our data are consistent with this view, and we will be further testing it in future equilibrium and kinetic experiments using site-directed mutants and the methodology presented here.

An important aspect of the insertion pathway is that the two pH-dependent transitions, W-to-W^+ and I-to-I^+, are not sequential but staggered; i.e., the second transition starts well before the first one is completed. This clearly follows from the insertion kinetics under conditions of incomplete binding (e.g., see kinetics measured at pH 6.5 in Figure 5). At the end of the insertion kinetic most of the membrane-associated T-domain is already inserted into the T-conformation, while a substantial fraction is still in solution. This additional protonation at the same pH can be explained by the change in the pK_a of titratable groups responsible for insertion (possibly E349 and D352) once they are brought from aqueous environment to the membrane interface. Protonation of titratable residues depends on dielectric properties of their environment and can be reasonably well predicted in soluble proteins from known structures (*40*, *41*). For membrane proteins, and especially for their lipid-exposed residues, such calculations are difficult and most likely will require extensive molecular dynamics simulations.

Experimental evidence indicates that the pK_a of anionic residues in peptides that interact with membranes at an acidic pH (e.g., GALA (*42*) or pHLIP (*43*)) is higher in membranes than in solution. A similar shift in protonation of carboxyl groups is responsible for flip-flop of a neutral form of fatty acids across the lipid bilayer (*44*). Consequently, the opposite effect, decreasing pK_a, can be expected for histidines, which is indeed observed experimentally for His-containing transmembrane peptides (*45*). In all of these cases, though, it is unclear whether the change in pK_a occurs in the hydrocarbon core of the bilayer or already on the membrane interface. In several systems, however, changes in protonation have been demonstrated to occur in the interfacial region of the bilayer. For example, it has been estimated that the pK_a of the C-terminus of model pentapeptides used to generate Wimley−White hydrophobicity scales shifts from 3.7 in aqueous buffer to 5.7 in the POPC interface (*46*). In addition, a study of a model membrane-binding peptide TMX-3 indicates that the pK_a of histidines can be shifted by 0.8 unit on uncharged lipid interfaces (*30*). It is not unreasonable to assume that a similar effect will manifest itself for acidic residues. Moreover, it is possible that their protonation will be affected by the presence of negative charges on the membrane, which would explain the promotion of insertion by anionic lipids reported here. We suggest that the existence of overlapping protonation transitions is an essential feature of all pH-driven membrane interactions.

Recently, we have demonstrated that membrane insertion of the T-domain, chaperoned by fluorinated surfactants, can be used for equilibrium thermodynamic studies experimentally addressing the issues related to understanding membrane protein stability (*27*). Here, we demonstrate how the diphtheria toxin T-domain can be used as a model for kinetic studies of insertion. Increasing evidence indicates that posttranslational insertions and changes in membrane topology are important features of folding (*47*−*50*) and possibly misfolding (*51*) of membrane proteins. But we know little of the free energy profiles along such transitions, due to the experimental challenges inherent in kinetic and thermodynamic studies with membrane proteins in

the cell. This study demonstrates the utility of the diphtheria toxin T-domain as a potentially useful experimentally accessible model system for using kinetic studies to reveal the physicochemical principles of alternating topology of membrane proteins.

ACKNOWLEDGMENT

We are grateful to Mr. M. A. Myers for editorial assistance. We thank the anonymous referees for valuable comments.

REFERENCES

1. Oh, K. J., Senzel, L., Collier, R. J., and Finkelstein, A. (1999) Translocation of the catalytic domain of diphtheria toxin across planar phospholipid bilayers by its own T domain. *Proc. Natl. Acad. Sci. U.S.A. 96*, 8467–8470.
2. Hoch, D. H., Romero-Mira, M., Ehrlich, B. E., Finkelstein, A., DasGupta, B. R., and Simpson, L. L. (1985) Channels formed by botulinum, tetanus, and diphtheria toxins in planar lipid bilayers: Relevance to translocation of proteins. *Proc. Natl. Acad. Sci. U.S.A. 82*, 1692–1696.
3. Neale, E. A. (2003) Moving across membranes. *Nat. Struct. Biol. 10*, 2–3.
4. Collier, R. J., and Young, J. A. (2003) Anthrax toxin. *Annu. Rev. Cell Dev. Biol. 19*, 45–70.
5. Bennett, M. J., and Eisenberg, D. (1994) Refined structure of monomeric diphtheria toxin at 2.3 Å resolution. *Protein Sci. 3*, 1464–1475.
6. Oh, K. J., Zhan, H., Cui, C., Hideg, K., Collier, R. J., and Hubbell, W. L. (1996) Organization of diphtheria toxin T domain in bilayers: A site-directed spin labeling study. *Science 273*, 810–812.
7. Oh, K. J., Zhan, H., Cui, C., Altenbach, C., Hubbell, W. L., and Collier, R. J. (1999) Conformation of the diphtheria toxin T domain in membranes: A site-directed spin-labeling study of the TH8 helix and TL5 loop. *Biochemistry 38*, 10336–10343.
8. Kachel, K., Ren, J. H., Collier, R. J., and London, E. (1998) Identifying transmembrane states and defining the membrane insertion boundaries of hydrophobic helices in membrane-inserted diphtheria toxin T domain. *J. Biol. Chem. 273*, 22950–22956.
9. Senzel, L., Gordon, M., Blaustein, R. O., Oh, K. J., Collier, R. J., and Finkelstein, A. (2000) Topography of diphtheria toxin's T domain in the open channel state. *J. Gen. Physiol. 115*, 421–434.
10. Zhao, G., and London, E. (2005) Behavior of diphtheria toxin T domain containing substitutions that block normal membrane insertion at Pro345 and Leu307: Control of deep membrane insertion and coupling between deep insertion of hydrophobic subdomains. *Biochemistry 44*, 4488–4498.
11. Wang, Y., Malenbaum, S. E., Kachel, K., Zhan, H. J., Collier, R. J., and London, E. (1997) Identification of shallow and deep membrane-penetrating forms of diphtheria toxin T domain that are regulated by protein concentration and bilayer width. *J. Biol. Chem. 272*, 25091–25098.
12. Chenal, A., Savarin, P., Nizard, P., Guillain, F., Gillet, D., and Forge, V. (2002) Membrane protein insertion regulated by bringing electrostatic and hydrophobic interactions into play. A case study with the translocation domain of the diphtheria toxin. *J. Biol. Chem. 277*, 43425–43432.
13. Ladokhin, A. S., Legmann, R., Collier, R. J., and White, S. H. (2004) Reversible refolding of the diphtheria toxin T-domain on lipid membranes. *Biochemistry 43*, 7451–7458.
14. Palchevskyy, S. S., Posokhov, Y. O., Olivier, B., Popot, J. L., Pucci, B., and Ladokhin, A. S. (2006) Chaperoning of insertion of membrane proteins into lipid bilayers by hemifluorinated surfactants: Application to diphtheria toxin. *Biochemistry 45*, 2629–2635.
15. Montagner, C., Perier, A., Pichard, S., Vernier, G., Menez, A., Gillet, D., Forge, V., and Chenal, A. (2007) Behavior of the N-terminal helices of the diphtheria toxin t domain during the successive steps of membrane interaction. *Biochemistry 46*, 1878–1887.
16. Posokhov, Y. O., Rodnin, M. V., Lu, L., and Ladokhin, A. S. (2008) Membrane insertion pathway of annexin B12: Thermodynamic and kinetic characterization by fluorescence correlation spectroscopy and fluorescence quenching. *Biochemistry 47*, 5078–5087.
17. Haugland, R. P. (1996) Handbook of Fluorescent Probes and Research Chemicals , 6th ed., Molecular Probes, Eugene, OR.
18. Ladokhin, A. S., Isas, J. M., Haigler, H. T., and White, S. H. (2002) Determining the membrane topology of proteins: Insertion pathway of a transmembrane helix of annexin 12. *Biochemistry 41*, 13617–13626.
19. Hope, M. J., Bally, M. B., Mayer, L. D., Janoff, A. S., and Cullis, P. R. (1986) Generation of multilamellar and unilamellar phospholipid vesicles. *Chem. Phys. Lipids 40*, 89–107.
20. Mayer, L. D., Hope, M. J., and Cullis, P. R. (1986) Vesicles of variable sizes produced by a rapid extrusion procedure. *Biochim. Biophys. Acta 858*, 161–168.
21. Bartlett, G. R. (1959) Phosphorus assay in column chromatography. *J. Biol. Chem. 234*, 466–468.
22. Posokhov, Y. O., and Ladokhin, A. S. (2006) Lifetime fluorescence method for determining membrane topology of proteins. *Anal. Biochem. 348*, 87–93.
23. Hess, S. T., Huang, S., Heikal, A. A., and Webb, W. W. (2002) Biological and chemical applications of fluorescence correlation spectroscopy: A review. *Biochemistry 41*, 697–705.
24. Rusu, L., Gambhir, A., McLaughlin, S., and Radler, J. (2004) Fluorescence correlation spectroscopy studies of peptide and protein binding to phospholipid vesicles. *Biophys. J. 87*, 1044–1053.
25. Rhoades, E., Ramlall, T. F., Webb, W. W., and Eliezer, D. (2006) Quantification of alpha-synuclein binding to lipid vesicles using fluorescence correlation spectroscopy. *Biophys. J. 90*, 4692–700.
26. Clamme, J. P., Azoulay, J., and Mely, Y. (2003) Monitoring of the formation and dissociation of polyethylenimine/DNA complexes by two photon fluorescence correlation spectroscopy. *Biophys. J. 84*, 1960–1968.
27. Posokhov, Y. O., Rodnin, M. V., Das, S. K., Pucci, B., and Ladokhin, A. S. (2008) FCS study of the thermodynamics of membrane protein insertion into the lipid bilayer chaperoned by fluorinated surfactants. *Biophys. J. 95*, L54–L56.
28. Perier, A., Chassaing, A., Raffestin, S., Pichard, S., Masella, M., Menez, A., Forge, V., Chenal, A., and Gillet, D. (2007) Concerted protonation of key histidines triggers membrane interaction of the diphtheria toxin T domain. *J. Biol. Chem. 282*, 24239–24245.
29. Ladokhin, A. S., Jayasinghe, S., and White, S. H. (2000) How to measure and analyze tryptophan fluorescence in membranes properly, and why bother? *Anal. Biochem. 285*, 235–245.
30. Ladokhin, A. S., and White, S. H. (2004) Interfacial folding and membrane insertion of a designed helical peptide. *Biochemistry 43*, 5782–5791.
31. Ladokhin, A. S., and White, S. H. (2001) Protein chemistry at membrane interfaces: Non-additivity of electrostatic and hydrophobic interactions. *J. Mol. Biol. 309*, 543–552.
32. Posokhov, Y. O., Gottlieb, P. A., Morales, M. J., Sachs, F., and Ladokhin, A. S. (2007) Is lipid bilayer binding a common property of inhibitor cysteine knot ion-channel blockers? *Biophys. J. 93*, L20–L22.
33. Ladokhin, A. S., and White, S. H. (1999) Folding of amphipathic α-helices on membranes: Energetics of helix formation by melittin. *J. Mol. Biol. 285*, 1363–1369.
34. Fernandez-Vidal, M., Jayasinghe, S., Ladokhin, A. S., and White, S. H. (2007) Folding amphipathic helices into membranes: Amphiphilicity trumps hydrophobicity. *J. Mol. Biol. 370*, 459–470.
35. Moore, J. W., and Pearson, R. G. (1981) Kinetics and Mechanism , 3rd ed., Wiley, New York.
36. Beechem, J. M. (1997) Picosecond fluorescence decay curves collected on millisecond time scale: Direct measurement of hydrodynamic radii, local/global mobility, and intramolecular distances during protein-folding reactions. *Methods Enzymol. 278*, 24.
37. Rodnin, M. V., Posokhov, Y. O., Contino-Pepin, C., Brettmann, J., Kyrychenko, A., Palchevskyy, S. S., Pucci, B., and Ladokhin, A. S. (2008) Interactions of fluorinated surfactants with diphtheria toxin T-domain: Testing new media for studies of membrane proteins. *Biophys. J. 94*, 4348–4357.
38. Lai, B., Zhao, G., and London, E. (2008) Behavior of the deeply inserted helices in diphtheria toxin T domain: helices 5, 8, and 9 interact strongly and promote pore formation, while helices 6/7 limit pore formation. *Biochemistry 47*, 4565–4574.
39. Ren, J., Sharpe, J. C., Collier, R. J., and London, E. (1999) Membrane translocation of charged residues at the tips of hydrophobic helices in the T domain of diphtheria toxin. *Biochemistry 38*, 976–984.
40. Khandogin, J., and Brooks, C. L.III (2006) Toward the accurate first-principles prediction of ionization equilibria in proteins. *Biochemistry 45*, 9363–9373.
41. Gordon, J. C., Myers, J. B., Folta, T., Shoja, V., Heath, L. S., and Onufriev, A. (2005) H++: A server for estimating pKas and adding missing hydrogens to macromolecules. *Nucleic Acids Res. 33*, W368–W371.
42. Li, W., Nicol, F., and Szoka, F. C.Jr. (2004) GALA: A designed synthetic pH-responsive amphipathic peptide with applications in drug and gene delivery. *Adv. Drug Deliv. Rev. 56*, 967–985.

43. Reshetnyak, Y. K., Segala, M., Andreev, O. A., and Engelman, D. M. (2007) A monomeric membrane peptide that lives in three worlds: In solution, attached to, and inserted across lipid bilayers. *Biophys. J. 93*, 2363–2372.
44. Kamp, F., and Hamilton, J. A. (2006) How fatty acids of different chain length enter and leave cells by free diffusion. *Prostaglandins, Leukotrienes Essent. Fatty Acids 75*, 149–159.
45. Bechinger, B. (1996) Towards membrane protein design: pH-sensitive topology of histidine-containing polypeptides. *J. Mol. Biol. 263*, 768–775.
46. Wimley, W. C., and White, S. H. (1996) Experimentally determined hydrophobicity scale for proteins at membrane interfaces. *Nat. Struct. Biol. 3*, 842–848.
47. Zhang, W., Bogdanov, M., Pi, J., Pittard, A. J., and Dowhan, W. (2003) Reversible topological organization within a polytopic membrane protein is governed by a change in membrane phospholipid composition. *J. Biol. Chem. 278*, 50128–50135.
48. Lu, Y., Turnbull, I. R., Bragin, A., Carveth, K., Verkman, A. S., and Skach, W. R. (2000) Reorientation of aquaporin-1 topology during maturation in the endoplasmic reticulum. *Mol. Biol. Cell 11*, 2973–2985.
49. Rapp, M., Granseth, E., Seppala, S., and von Heijne, G. (2006) Identification and evolution of dual-topology membrane proteins. *Nat. Struct. Mol. Biol. 13*, 112–116.
50. Bogdanov, M., Xie, J., and Dowhan, W. (2009) Lipid-protein interactions drive membrane protein topogenesis in accordance with the positive inside rule. *J. Biol. Chem. 284*, 9637–9641.
51. Sanders, C. R., and Myers, J. K. (2004) Disease-related misassembly of membrane proteins. *Annu. Rev. Biophys. Biomol. Struct. 33*, 25–51.